Initiation Mechanism of Meso-β Scale Convective Systems

Peng Jiayi (彭加毅)[1,2①], Wu Rongsheng (伍荣生), and Wang Yuan (王 元)

[1]*Key Laboratory of Mesoscale Severe Weather, Ministry of Education, China*

Department of Atmospheric Sciences, Nanjing University, Nanjing 210093

[2]*Department of Atmospheric Science, Nanjing Institute of Meteorology, Nanjing*, 210044

(Received September 11, 2001; revised July 8, 2002)

ABSTRACT

With the aid of the Penn State-NCAR MM5 model, the initiation mechanism of meso-β scale convective systems (MCS) is investigated on the basis of simulation of the temporal and spatial thermodynamic structure of the MCS that occurred in Wuhan, Hubei, China and its surrounding area on 21 July 1998. Using the PV inversion method, comparisons among the upper-, middle-, and low-level tropospheric potential vorticity (PV) perturbations, as well as their effects on the initiation of MCS, indicate that the low-level tropospheric PV perturbations play an important role in the triggering of MCS. Further analysis reveals that the interaction between the southwest low-level jet and the gravity-inertia wave indeed initiates MCS in the conditionally unstable ambient atmosphere.

Key words: mesoscale, convective systems, low-level jet, Gravity-inertia wave

1. Introduction

The initiation of meso-scale convective systems (MCS) has been intensively studied by many researchers, among others, Chen et al. (1998) and Chen (2000) dealt with a series of convective rainstorms developed successively along the Mei-yu front on 12-13 June 1991 by using the Penn State-NCAR Meso-scale Model Version 5. It turned out that the initiation of MCS along the Mei-yu front may be a barotropic process with respect to the character of a weak temperature gradient and strong wind shear across the front. Particularly, Chen et al. (1998) demonstrated that the initial development of the mid-level cloud at $Z=5$ km results from the interaction of the upper-level ageostrophic circulation with the mid-level moist layer. The analysis of Cheng and Feng (2001) also identified that the abrupt, extraordinarily heavy rainfall in 1998 was in close relationship with the short-wave trough at 500 hPa and the low vortex with shear line at 700 hPa, as well as with the successive generation and intense development of MCS along the shear line. In another study, the characteristics of the synoptic background and meso-scale evolution process of the extremely heavy rain that successively took place along the Yangtze River valley in China's eastern Province of Hubei during 21-22 July 1998 were analyzed by Hu et al. (2001). Their results suggested that the gravity-inertia wave energy dispersion in the upper-level troposphere was the possible mechanism of the severe storm. On the other hand, Sun and Zhai (1980) and Sun (1985) illustrated that some short-period waves which are closely related to the non-geostrophic wind of the axis often occur on the jet. The waves corresponding to the temperature and pressure disturbances propagate along the axis and cause the sharp development of convection and the formation of

①E-mail: jiaypeng@nju.edu.cn

heavy rain clusters.

From the above discussion, it is clear that many factors exist that initiate MCS. In fact, the southwest low-level jet (LLJ) plays an important role in the transport of vapour and momentum, and so it should be the key factor in the initiation of the MCS that happened in the southwest part of Hubei in 1998. That is the beginning point of this paper. Mainly through the numerical replication of the real MCS case that occurred in Hubei on 21 July 1998, the crucial factor in the triggering mechanism will be identified. Furthermore, by virtue of PV inversion (Davis 1992; Davis and Emanuel 1991), the comparisons among the upper-, middle-, and low-level tropospheric potential vorticity (PV) perturbations in the formation of MCS are implemented so that the interaction of the LLJ and gravity-inertia wave associated with the initiation of MCS will be made clear.

2. Overview of the synoptic situation

From 2000 BST (Beijing Standard Time) 20 July 1998 to 2000 BST 22 July 1998, an extraordinarily heavy rainfall occurred over Hubei. Two meteorological observatories, Huangshi and Wuhan, recorded severe rainfall of 499 mm and 457 mm respectively in 48 hours. Observed 24-hour rainfall ending at 2000 BST 21 July over Wuhan city was up to 286 mm (see Fig. 3a), with a recorded 1-hour rainfall 88.4 mm breaking the historical record (National Meteorological Center and National Satellite Meteorological Center 1999).

By virtue of the three-time-mean (0200, 0800, and 1400 BST) National Centers for Environmental Prediction (NCEP) data on 21 July 1998, the geopotential height and wind distribution at 850 hPa, 500 hPa, and 200 hPa are displayed in Fig. 1. In the 500 hPa chart, a 'Single Blocking Pattern' is located to the north of Baikal Lake (53°N, 107°E) with two lows (the Balkash Lake Low and Northeast Low) to the south of it. The cold current moves southward from the rears of the two lows. The southwest low vortex at 850 hPa lies in the western flank of the shear line; south of which, it is the southwest LLJ that enhances the convergence of the cold / warm current. At 200 hPa, a strong divergence area lies on the eastern side of the South-Asia High. Because the southeastern part of Hubei is just situated on the shear line and in the left-front quadrant of the jet axis, it was vulnerable to the eruption of a severe storm.

3. Mesoscale model and experimental design

The Penn State-NCAR MM5 model was used to carry out a numerical simulation of the meso-β scale convective system that appeared in the Wuhan area. The MM5 model is a non-hydrostatic, primitive equation model with a terrain-following vertical coordinate. The model physics used in this experiment includes the Reisner Graupel for resolvable-scale motion and the subgrid-scale convection of Grell's cumulus parameterization scheme. Blackadar's high-resolution planetary boundary layer (PBL) scheme was implemented to calculate the vertical fluxes of sensible heat, latent heat, and momentum and turbulent mixing in the PBL. A detailed description of MM5 can be found in Dudhia (1993) and Grell et al. (1994).

The design of the two-way nesting model domains is shown in Fig.2a. They consist of a 20-km grid (D02, mesh size of 61 × 61) and a 60-km grid (D01, mesh size of 80 × 92). Both grids have 23 vertical levels. Figure 2b displays the terrain height for domain 2, with line AB used for Fig. 8 and Fig. 10, and point C (112.7°E, 28.1°N) for Fig. 11.

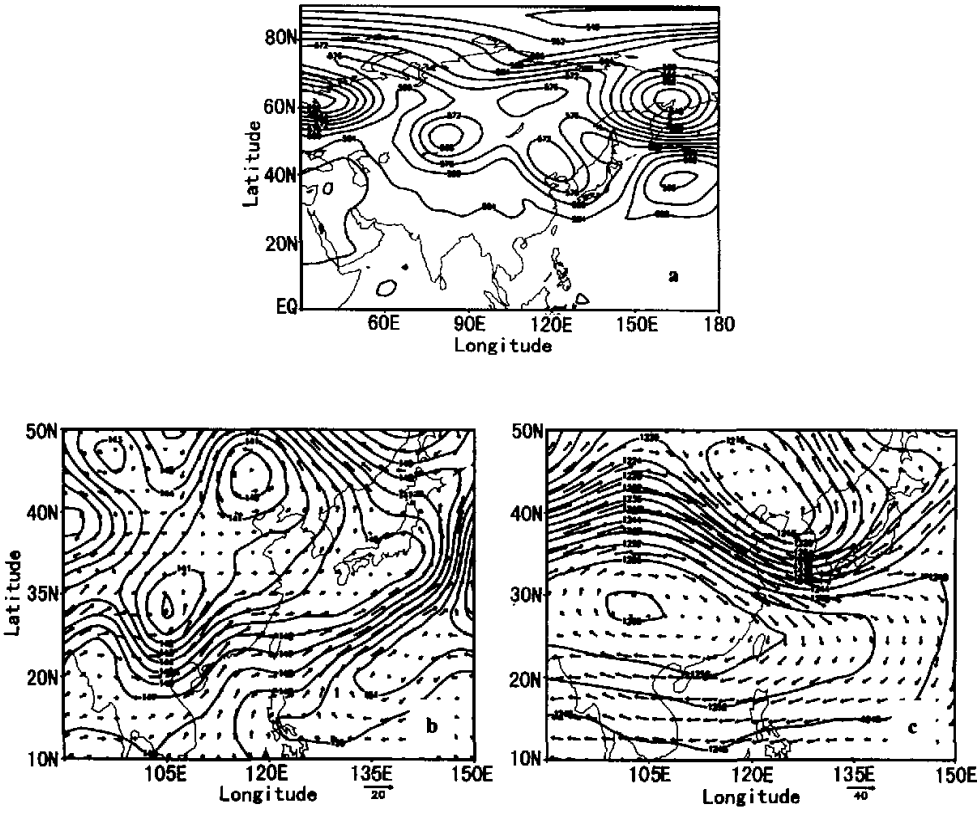

Fig. 1. The three-time mean (0200, 0800, and 1400 BST 21 July 1998) geopotential height (solid lines, 10 gpm) and wind (arrows, m s^{-1}) fields at (a) 500 hPa, (b) 850 hPa, and (c) 200 hPa. Shading indicates the jet stream.

The dataset from the NCEP global analysis archives with 2.5° × 2.5° latitude–longitude resolution (which are interpolated to the model grid point locations) has been employed in the model initialization as the first guess fields, which are then enhanced by blending in observational data using an objective analysis technique to introduce meso-scale features. The temporal lateral boundary condition is provided by repeating the above procedure at 6-hour intervals. The time period of interest is from 0800 BST 20 to 0800 BST 23 July 1998. This paper will focus on the results of the 20-km grid (Domain 02).

4. Model verification

In this section, we verify the 24-hour simulation of the meso-β scale convective system, mainly from Domain 02 with 20-km resolution, against various observations (e.g., surface rainfall analysis and satellite imagery). The next section will be devoted to the initiation

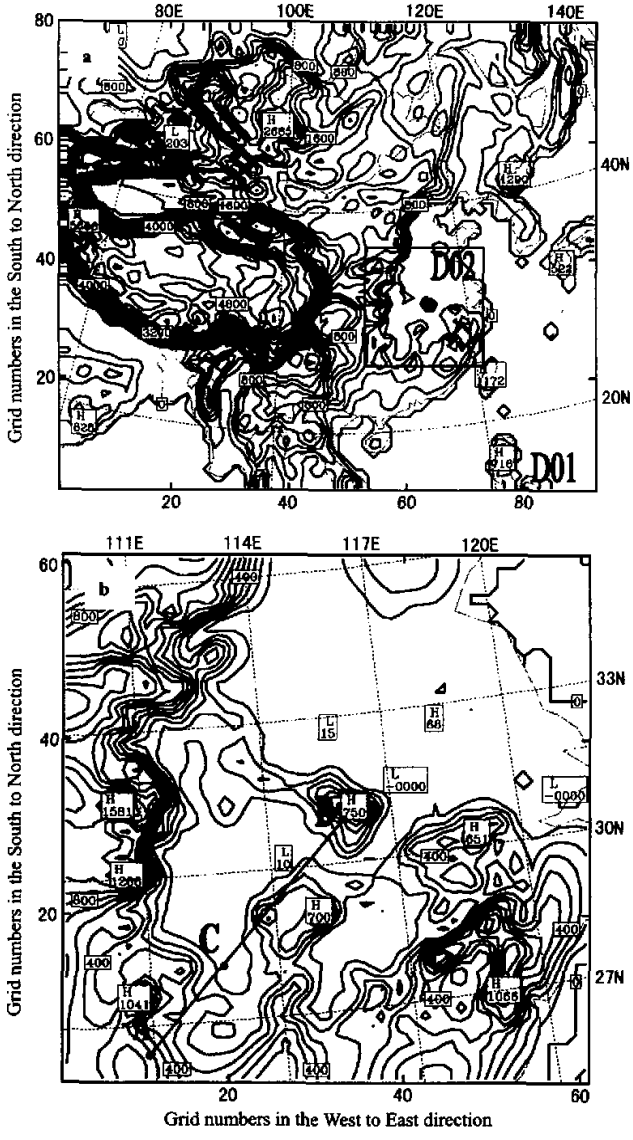

Fig. 2. (a) The two-way nesting model domains. (b) The terrain heights of Domain 02. The line AB shows the position of the vertical cross sections shown in Figs. 8 and 10, and C indicates the position (112.7°E, 28.1°N) in Fig. 11.

of MCS.

The comparison between the simulated and the observed 24-hour accumulated rainfall over Hubei is shown in Fig.3. The simulted heavy rainfall center is situated slightly to the southeast of the observed, with the rainfall intensity (150 mm) under-predicted. Generally,

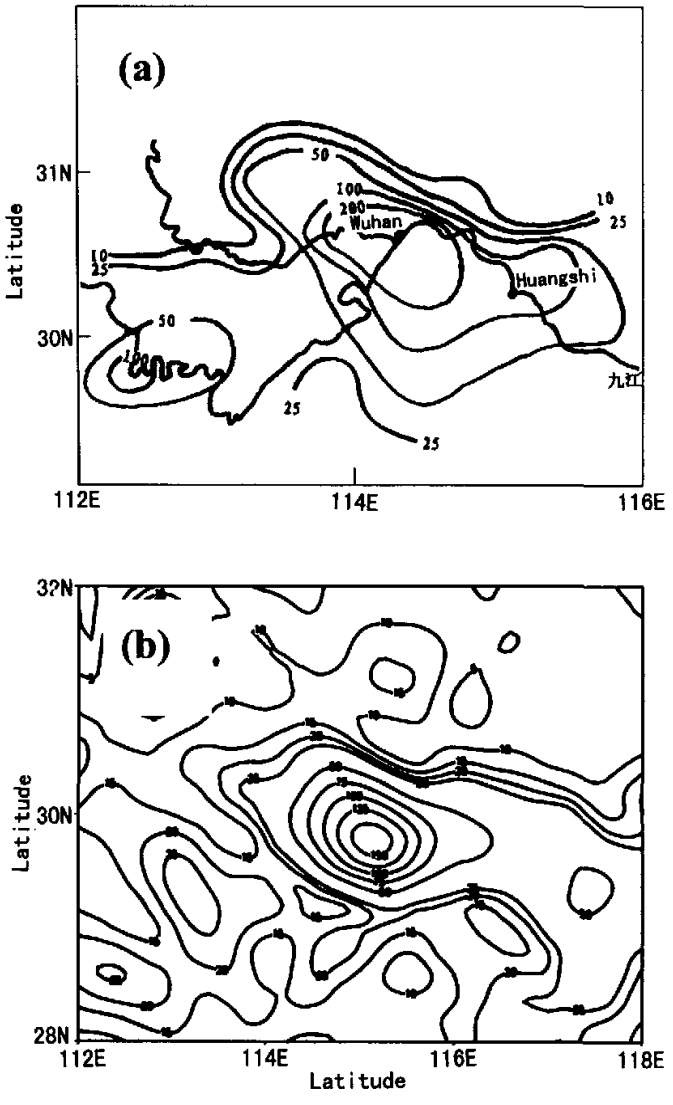

Fig. 3. (a) Observed 24-h rainfall from 2000 BST 20 July to 2000 BST 21 July 1998. (b) Simulated 24-h rainfall. Rainfall contours are in mm.

the simulation depicts the main features of the observed heavy rainfall in terms of location and intensity. To judge the simulation of the severe storm, further verification is taken by comparing the structure of MCS (Fig.4) and the Geostationary Meteorological Satellite (GMS) infrared (IR) images (Fig. 5). At 0400 BST 21 July, shallow convection emerged to the north of Muohu Mountain (30°N), similar to features of the observed IR imagery. Three

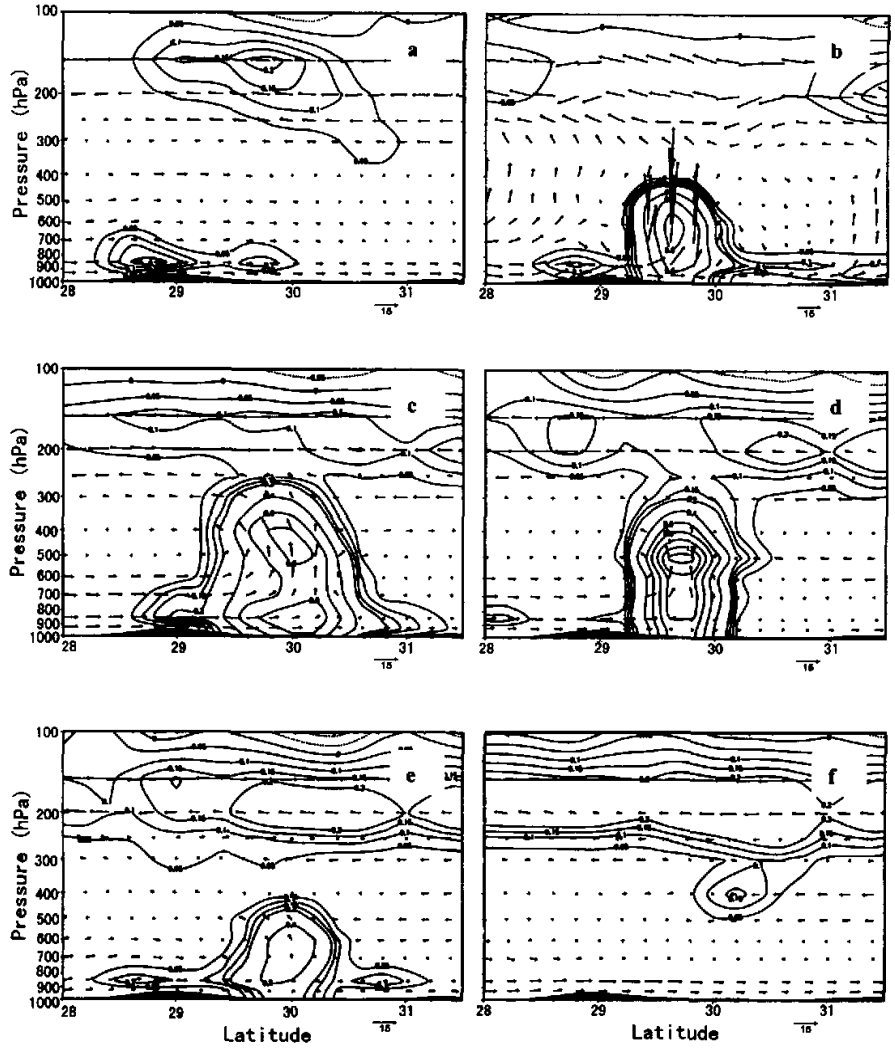

Fig. 4. The latitude–height cross section along 115°E of the mean meridional and vertical wind vector (arrows) and the total cloud water (solid lines and shaded areas) at (a) 0400 BST, (b) 0700 BST, (c) 1000 BST, (d) 1300 BST, (e) 1600 BST, and (f) 1900 BST, 21 July 1998. The abscissa indicates latitude (°N) and the ordinate height (hPa).

hours later, the convection moved northward, and the extraordinarily strong convection does abruptly erupt, accompanied by the formation of the MCS, which is in agreement with the strong convection displayed in the IR imagery at 0700 BST. The MCS continue to be intensified up to 1000BST. After that, the MCS begin to decay with time, dying away at 1900 BST. Comparison between Fig.4 and Fig.5 shows that the temporal evolution of the simulated

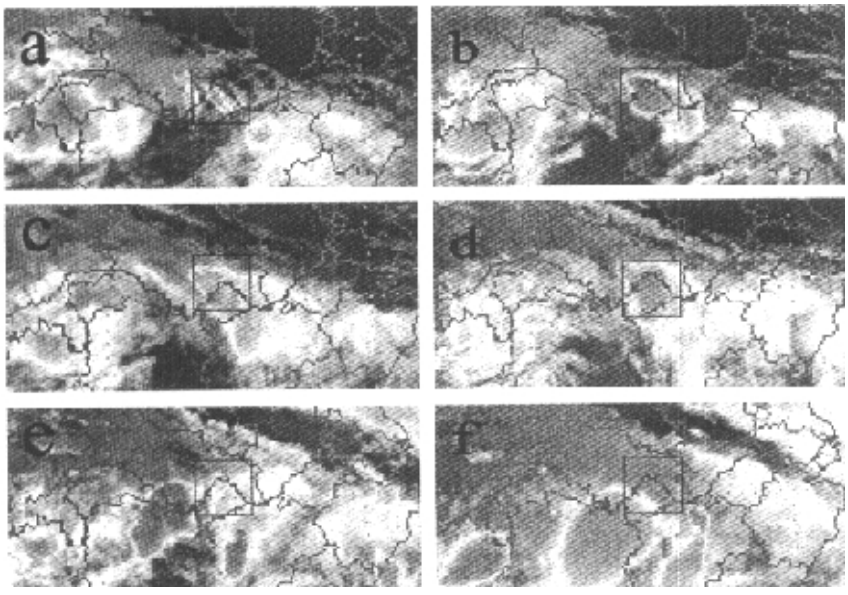

Fig. 5. GMS infrared satellite images for (a) 0400 BST, (b) 0700 BST, (c) 1000 BST, (d) 1300 BST, (e) 1600 BST, and (f) 1900 BST, 21 July 1998. The box indicates the southeastern part of Hubei Province.

MCS is in harmony with the variation of IR satellite images.

5. Initiation mechanism of MCS

The previous section has demonstrated that we have simulated the temporal variation of MCS with the aid of MM5 model. In this section we will focus on the initiation of MCS. From the latitude–height cross section of equivalent potential temperature θ_e along 115°E at 0400 BST 21 July 1998 (for the sake of simplicity, figure omitted), conditionally unstable lapse rates are observed, which produce the suitable condition most favorable for the formation of strong convection. Nevertheless, one question remains to be answered, namely what is the key factor in the initiation of MCS. Here we seek the answer through employing the PV inversion method in order to compare the effects of the upper–, middle–, and low–level tropospheric potential vorticity (PV) perturbations on the initiation of MCS.

5.1 *Potential vorticity inversion*

To assess the effects of different physical process in the evolution of the eruption of MCS, we use Davis et al. (1991, 1992) piecewise Ertel's potential vorticity perturbations (EPVP) inversion technique by partitioning the EPVP in the concerned domain into several anomaly components in order to find the contribution of each component to the wind

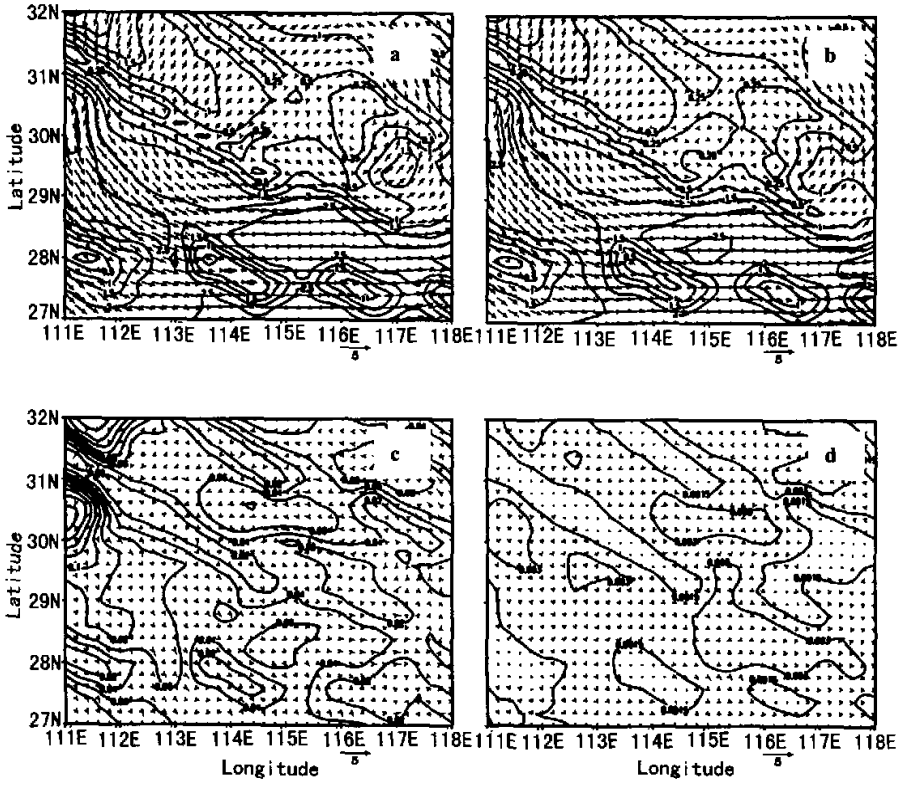

Fig. 6. The contributions of (a) q'_{tot}, (b) q'_{low}, (c) q'_{mid}, and (d) q'_{upp} to the 850 hPa wind anomaly at 0400 BST 21 July 1998. The solid lines indicate the streamlines and the dashed lines the wind speed contours.

anomaly (i.e., the departure from period mean).

First of all, we compute the Ertel's potential vorticity (EPV) by

$$q = \frac{1}{\rho}\eta \cdot \nabla\theta,$$

in which η is the absolute vorticity vector, θ the potential temperature, and ρ the density. The perturbations of EPV (q') are specified as the departure from the mean of the period 2100 BST 20 July to 2000 BST 21 July. The effects of the total EPVP (q'_{tot}) are divided into three parts: (a) the low-level tropospheric effect, which is represented by the large EPVP ($q' \geqslant 0$) tropospheric (1000–800 hPa) air, denoted by q'_{low}; (b) the middle-level tropospheric effect, where EPVP is denoted by q'_{mid}, which represents the 700–500 hPa tropospheric EPVP ($q' \geqslant 0$); and (c) the upper-level tropospheric effect, where EPVP is the same as (b) but for 400–200 hPa, EPVP represented by q'_{upp}.

The contributions of q'_{tot}, q'_{low}, q'_{mid}, and q'_{upp} to the 850 hPa wind anomaly at

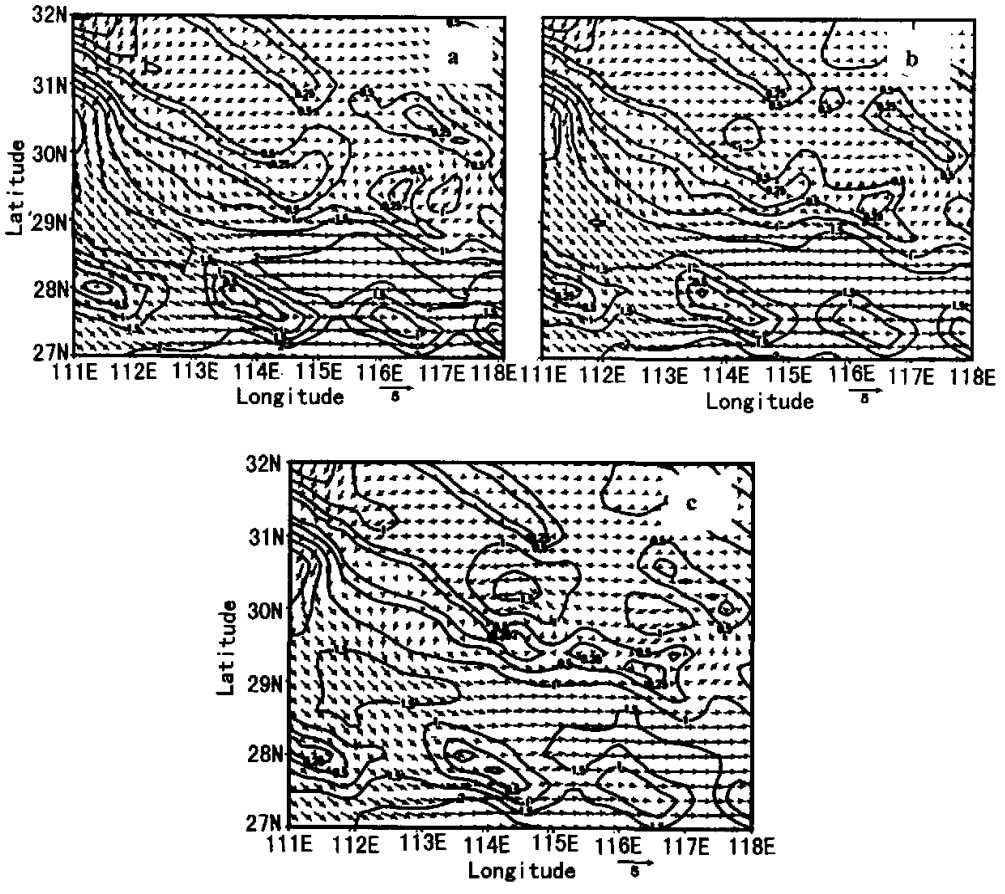

Fig. 7. The contribution of q'_{low} to the 850 hPa wind anomaly at (a) 0500 BST, (b) 0600 BST, and (c) 0700 BST 21 July 1998. The solid lines indicate the streamlines and the dashed lines the wind speed contours.

0400 BST 21 July 1998 have been illustrated in Fig. 6. Comparison between Fig. 6a and Fig. 6b indicates that a cyclonic shear is located around the given point of (30°N, 114.5°E), and in this area the q'_{low} and / or q'_{tot} contributions to wind speed anomaly (0.25 m s^{-1}) are similar to each other. The wind speed anomaly of q'_{mid} (0.02 m s^{-1}, see Fig. 6c) is less than one-tenth of the value of q'_{low}, and the wind speed anomaly for q'_{upp} (0.0015 m s^{-1}, see Fig. 6d) is smaller than that of q'_{mid}. From PV inversion analysis at other times, for instance, 0500 BST, 0600 BST, and 0700 BST, the same results can be obtained (figure omitted).

From the contribution of q'_{low}, to the 850 hPa wind anomaly at 0500 BST, 0600 BST, and 0700 BST 21 July 1998, we can see the cyclonic shear emerging in the location (30°N, 114.5°E) at 0500 BST, with the formation of cyclonic circulation at 0600 BST, and a

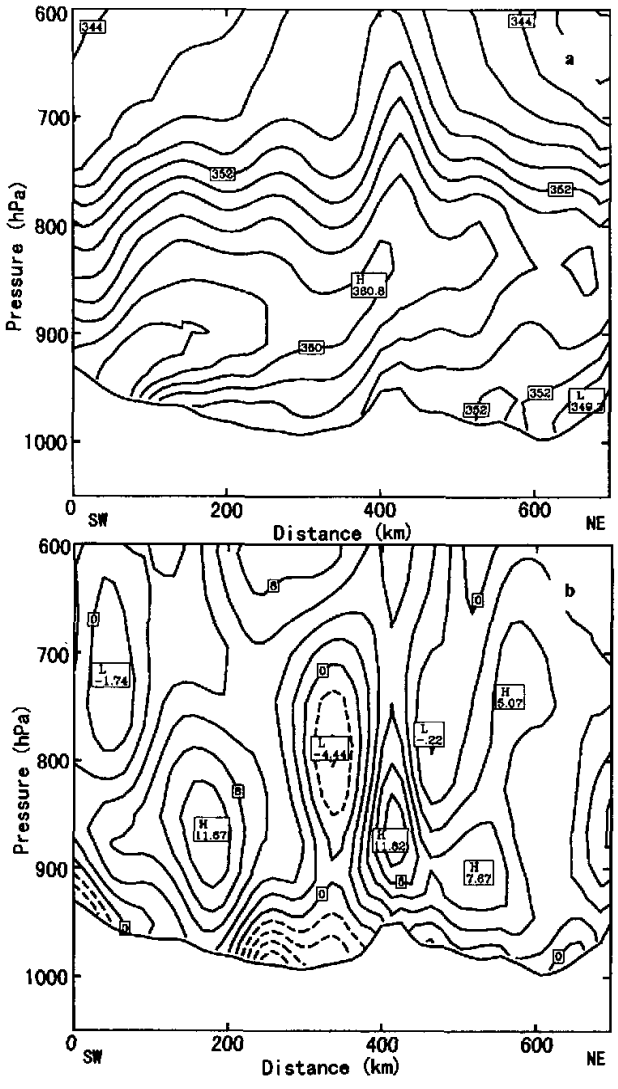

Fig. 8. The vertical cross section of (a) equivalent potential temperature θ_e (K) and (b) ageostrophic wind (m s^{-1}) along the line AB (cf. Fig. 2b) at 0300 BST 21 July 1998. A positive ageostrophic wind indicates a southwest wind and negative values a northeast wind.

strengthened cyclone at 0700 BST. At this time, the strong convection erupts, accompanied by two large wind anomaly centers (1.5 m s^{-1}) which are located to the north and the southeast sides of the cyclone. The foregoing discussion demonstrates that the low-level PV perturbation plays an important role in the initiation of MCS.

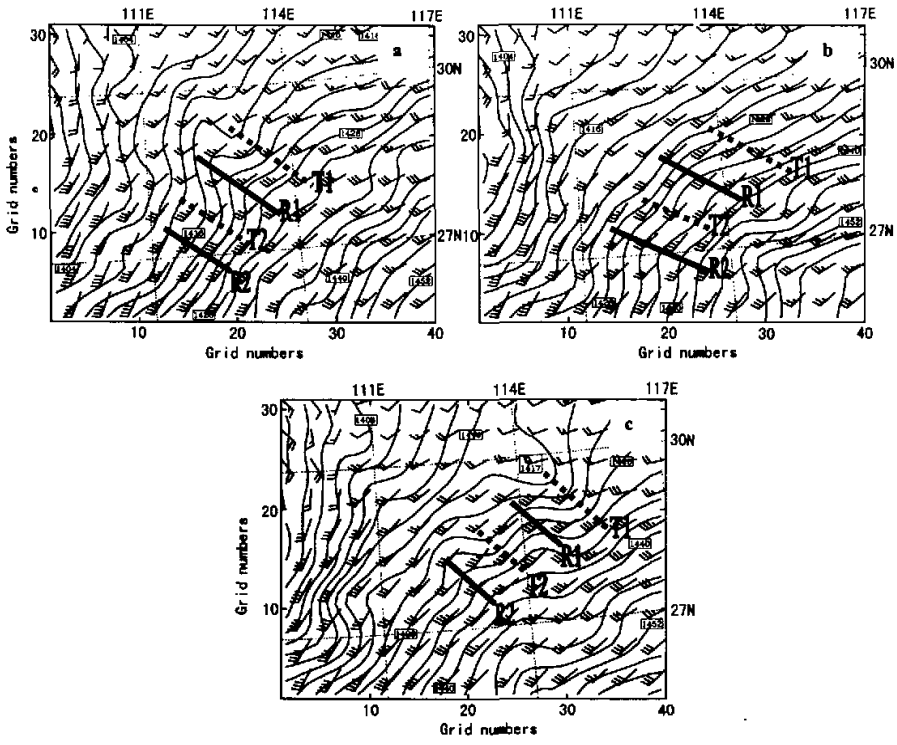

Fig. 9. The 850 hPa horizontal wind vector and geopotential height at (a) 0300 BST, (b) 0500 BST, and (c) 0700 BST, 21 July 1998. "T" denotes the axis of a height trough and "R" the axis of a height ridge.

5.2 *The interaction between the southwest low-level jet and the gravity-inertia wave*

It is well known that the southwest low-level jet plays an important role in the transport of vapour and momentum. The ageostrophic wind in the low-level jet under some conditions cannot adjust itself to the geostrophic balance, and therefore instability of the gravity-inertia wave must occur. Consequently, the interaction between southwest low-level jet and the gravity-inertia wave might be the crucial factor in the triggering of MCS.

Figure 8 displays the vertical cross section of equivalent potential temperature θ_e and ageostrophic wind along the line AB (see Fig. 2b) at 0300 BST 21 July 1998. The warm center ($\theta_e > 360$ K) at 900 hPa indicates an inversion layer in the lower troposphere. The corresponding ageostrophic wind component demonstrates strong ageostrophic features in the vicinity of the low-level jet at 850–900 hPa (see Fig. 10), with a maximum ageostrophic wind speed of 12 m s^{-1}. The ageostrophic wind was also separated by positive centers (southwest wind) and negative centers (northeast wind) in the interval, accompanied by obvious convergence / divergence and the corresponding vertical motion; this is favorable for the generation and propagation of the gravity-inertia wave through the geostrophic adjustment

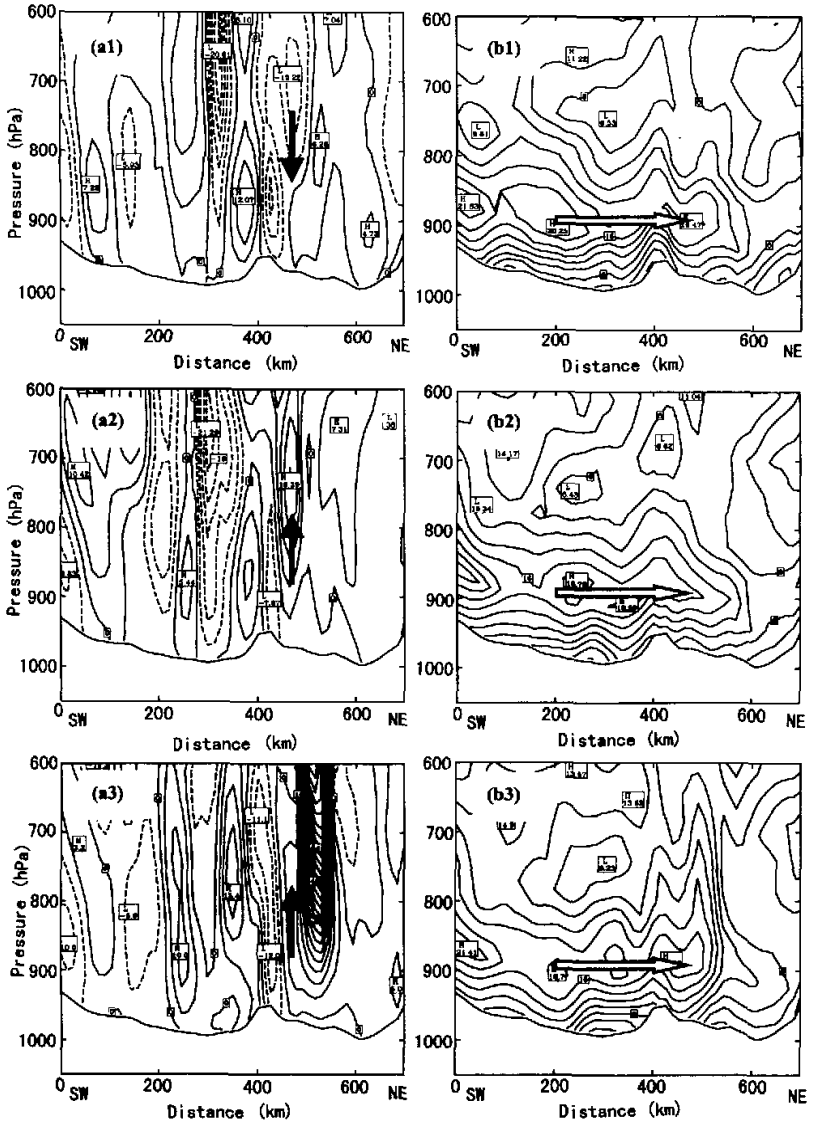

Fig. 10. Vertical cross section of vertical motion (a1, a2, and a3) and the horizontal wind speed (b1, b2 , and b3) along line *AB* (see Fig. 2b) at 0300 BST, 0500 BST, and 0700 BST 21 July 1998, respectively. The vertical motion is contoured at 4–cm s^{-1} intervals, with soid lines for updraft and dashed lines for downdraft. The solid arrow indicates the vertical motion in the southeast part of Hubei Province. The open arrow in panels b1, b2, and b3 denotes the low–level jet.

processes under the condition of an inversion layer. Blumen (1972) showed that the Rossby radius of deformation (hence, the gravity–inertia wavelength) in a stratified atmosphere is

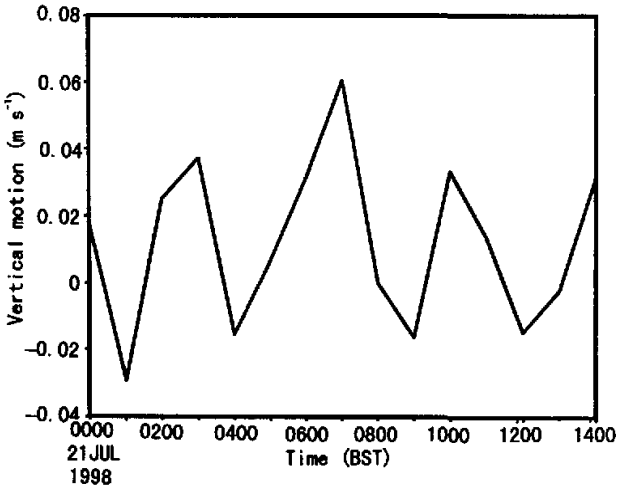

Fig. 11. The temporal variation of vertical motion at piont C (112.7°E, 28.1°N) (cf. Fig. 2b) during the period 0000–1400 BST 21 July 1998. Units: cm s^{-1}.

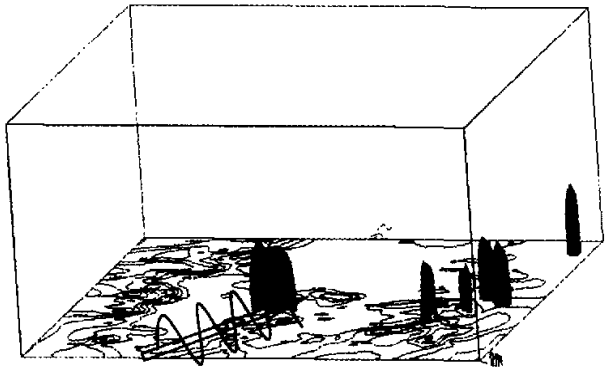

Fig. 12. Schematic diagram of the initiation of a meso-β scale convective system with respect to the interaction of the southwest low-level jet and the gravity-inertia wave. The contour lines indicate terrain height. The shaded area displays severe convection, to the north of which is Dabe mountain and the south one for Muohu mountain. The heavy arrow indicates the southwest low-level jet and the wave-like curve the gravity-inertia wave.

given by

$$\lambda_N \approx \frac{NH}{2\pi f},$$

where the Brunt-Väisälä frequency is $N = 1.0 \times 10^{-2} s^{-1}$, H is the atmosphere scale height

(H=8 km), and f the Coriolis parameter (f= 0.7511× 10^{-4} s^{-1}), so that the gravity–inertia wavelength is around λ = 170 km.

The horizontal structure of the gravity–inertia waves can be seen from the distribution of the 850 hPa geopotential height and wind (Fig. 9). The gravity–inertia waves propagate along the southwest LLJ, and at 0700 BST, arrive at the southeast part of Hubei and initiate the meso–β scale low–pressure system. Also, we can indicate the vertical structure of the gravity–inertia waves from the southwest–northeast vertical cross section of the vertical motion (w) and the horizontal wind speed along line AB (Fig. 10). The propagation of the gravity–inertia waves is evident through the low–level troposphere. The adjacent updraft (or downdraft) centers suggest a 150 km wavelength for the gravity–inertia wave, which is coordinated with the wavelength based on geostrophic adjustment theory (in the previous paragraph). From the vertical motion over the southeast part of Hubei, we can see a downdraft emerges in the low–level troposphere at 0300 BST, with a weak updraft (16 cm s^{-1}) at 0500 BST and a strong updraft (96 cm s^{-1}) at 0700 BST, corresponding with the eruption of the severe convective system.

The horizontal wind speed of up to 20 m s^{-1} indicates a southwest low–level jet at 850–900 hPa. The low–level jet presents a few large wind cores, indicating its interaction with the gravity–inertia wave. Comparison with the distributions at 0500 BST and 0700 BST reveals that the enhanced low–level jet cores move northeastward, initiating the severe storm. The temporal variation of vertical motion at point C (112.7°E, 28.1°N) suggests an approximate 3–hour period for the gravity–inertia wave (see Fig.11), from which we can calculate its propagation speed (14 m s^{-1}). This figure coincides with the results of Uccellini and Koch (1987). The foregoing analysis indicates the southwest low–level jet / gravity–inertia wave interaction initiates the meso–scale convective system.

6. Conclusion

The temporal and spatial thermodynamic structure of the meso–β scale convective system situated in the area of Wuhan on 21 July 1998 is successfully replicated by the implementation of the Penn State–NCAR MM5 model, and its initiation mechanism is investigated in detail by PV inversion. Comparison with the effect of upper–, middle–, and low–level tropospheric potential vorticity (PV) perturbations on the initiation of MCS in the context of PV inversion indicates that the low–level tropospheric PV perturbation is the essential factor in the eruption of MCS. Further analysis reveals that the southwest low–level jet / gravity–inertia wave interaction initiates MCS in the conditionally unstable atmosphere (Fig. 12). It is evident that there exists a non–linear interaction between the topographic gravity wave and the gravity–inertia wave induced by the shear instability of the southwest low–level jet. Further dynamical research will be implemented in the future to obtain insight into the non–linear interaction processes. In the meantime, more observational data are needed to verify the features of the gravity–inertia wave.

Acknowledgments. The authors are very grateful to Prof. Tan Zhemin, Dr. Fang Juan, Dr. Xiang Jie, and Dr. Wang Chunming for their beneficial discussions. We are deeply indebted to the reviewers for their helpful comments and criticism on an earlier manuscript. This work was sponsored by the Nanjing University Postdoctoral Foundation, the Science Foundation of Jiangsu Province Education Bureau (00KJB170001) and NSF of Jiangsu (BK99020), the State Key Basic Program: CHERES, and the National Natural Science Foundation of China under Grant No. 40075011.

REFERENCES

Blumen, W., 1972: Geostrophic adjustment. *Rev. Geophys. Space Phys.*, **10**, 485–528.

Chen Shoujun, Yinghwa Kuo, Wei Wang, Zuyu Tao, and Bo Cui, 1998: A modeling case study of heavy rainstorms along the Mei-yu front. *Mon. Wea. Rev.*, **126**, 2330–2351.

Chen Shoujun, 2000: The mesoscale convective system on Mei-yu front. *Proceedings of the National Key Programme for Developing Basic Sciences (CHERES)*, Dalian, P.R. China 8–12 May 2000, pp17.

Chen Chiang, Weikuo Tao, Payliam Lin, George S. Lai, S.F. Tseng, and Taichi Chen Wang, 1998: The intensification of the low-level jet during the development of mesoscale convective systems on a Mei-yu front. *Mon. Wea. Rev.*, **126**, 349–371.

Cheng Linsheng, and Feng Wuhu, 2001: Analyses and numerical simulation on an abrupt heavy rainfall and structure of a mesoscale vortex during July 1998. *Chinese Journal of Atmospheric Sciences*, **25**, 465–478.

Davis, C. A., 1992: Piecewise potential vorticity inversion. *Journal of the Atmospheric Sciences*, **49**, 1397–1411.

Davis, C. A., and K. A. Emanuel, 1991: Potential vorticity diagnostics of cyclogenesis. *Mon. Wea. Rev.*, **119**, 1929–1953.

Dudhia, J., 1993: A nonhydrostatic version of the Penn State–NCAR mesoscale model: Validation tests and simulation of an Atlantic cyclone and the cold front. *Mon. Wea. Rev.*, **121**, 1493–1513.

Grell, G. A., J. Dudhia, and D. R. Stauffer, 1994: A description of the fifth-generation Penn State / NCAR Mesoscale Model (MM5). NCAR / TN-398+STR NCAR TECHNICAL NOTE, 1–121.

Hu Bowei, Cui Chunguang, and Fang Chunhua, 2001: Causes of a two-day successively extremely heavy rain along the Changjiang Valley in the eastern Hubei Province during 21–22 July 1998. *Chinese Journal of Atmospheric Sciences*, **25**, 479–491.

National Meteorological Center and National Satellite Meteorological Center, 1999: The mesoscale analyses of "98.7" successively extremely heavy rain in the southeastern Hubei Province. *'98 Severe Flood in China and Weather Prediction*, China Meteorological Press, Beijing, 181–182.

Sun Shuqing, and Zhai Guoqing, 1980: On the instability of the low level jet and its trigger function for the occurrence of heavy rainstorms. *Chinese Journal of Atmospheric Sciences*, **4**, 327–337.

Sun Shuqing, 1985: Gravity waves on the axis of low level jet and their instability. *Advances in Atmospheric Sciences*, **2**, 112–123.

Uccellni, L.W., and S. E. Koch, 1987: The synoptic setting and possible energy sources for mesoscale wave disturbances. *Mon. Wea. Rev.*, **115**, 721–729.

β中尺度对流系统的触发机制

彭加毅　伍荣生　王　元

摘　要

利用MM5 V3.4模式再现了"98.7"武汉及其临近地区β中尺度对流系统的时空4维结构，在此基础上讨论β中尺度对流系统的触发机制。应用位涡反演理论对比分析对流层上层、中层及下层位涡扰动对β中尺度对流系统形成的作用，得出对流层下层位涡扰动为该β中尺度对流系统爆发的主要因子，进而分析指出，在大气为条件性不稳定层结情况下，西南低空急流与重力波相互作用导致β中尺度对流系统的爆发。

关键词：β中尺度对流系统，低空急流，重力波